Cardiovascular Engineering and Technology, Vol. 2, No. 4, December 2011 *(© 2011)* pp. 408–425
DOI: 10.1007/s13239-011-0065-3

An Efficient R-peak Detection Based on New Nonlinear Transformation and First-Order Gaussian Differentiator

P. KATHIRVEL,[2] M. SABARIMALAI MANIKANDAN,[1] S. R. M. PRASANNA,[3] and K. P. SOMAN[2]

[1]Department of Electronics and Communication Engineering, Amrita School of Engineering, Amrita Vishwa Vidyapeetham, Coimbatore 641105, India; [2]Center for Excellence in Computational Engineering and Networking, Amrita Vishwa Vidyapeetham, Coimbatore, Tamilnadu, India; and [3]Department of Electrical and Electronics Engineering, Indian Institute of Technology Guwahati, Guwahati, Assam, India

(Received 18 May 2011; accepted 27 September 2011; published online 12 October 2011)

Associate Editor Ajit P. Yoganathan oversaw the review of this article.

Abstract—In this paper, we present a reliable and efficient automatic R-wave detection based on new nonlinear transformation and simple peak-finding strategy. The detection algorithm consists of four stages. In the first stage, the bandpass filtering and differentiation operations are used to enhance QRS complexes and to reduce out-of-band noise. In the second stage, we introduce a new nonlinear transformation based on energy thresholding, Shannon energy computation, and smoothing processes to obtain a positive-valued feature signal which includes large candidate peaks corresponding to the QRS complex regions. The energy thresholding reduces the effect of spurious noise spikes from muscle artifacts. The Shannon energy transformation amplifies medium amplitudes and results in small deviations between successive peaks. Therefore, the proposed nonlinear transformation is capable of reducing the number of false-positives and false-negatives under small-QRS and wide-QRS complexes and noisy ECG signals. In the third stage, we propose a simple peak-finding strategy based on the first-order Gaussian differentiator (FOGD) that accurately identifies locations of candidate R-peaks in a feature signal. This stage computes convolution of the smooth feature signal and FOGD operator. The resultant convolution output has negative zero-crossings (ZCs) around the candidate peaks of feature signal due to the anti-symmetric nature of the FOGD operator. Thus, these negative ZCS are detected and used as guides to find locations of real R-peaks in an original signal at the fourth stage. Unlike other existing algorithms, the proposed algorithm does not use search back algorithm and learning phase. The proposed algorithm is validated using the standard MIT-BIH arrhythmia database and achieves an average sensitivity of 99.94% and a positive predictivity of 99.96%. Experimental results show that the proposed algorithm outperforms other existing algorithms in case of different QRS complex morphologies (negative, low-amplitude, wide), very big change in amplitudes of adjacent R-peaks, irregular heart rates, and noisy ECG signals.

Keywords—ECG signal analysis, QRS complex detection, ECG beat recognition, Heart rate variability analysis, Shannon energy, Gaussian differentiator, Peak finding logic.

INTRODUCTION

Automatic R-peak detection algorithm is essential for many types of ECG applications including heart rate monitor (HRM), ECG wave delineator, fetal heart rate monitor (fHRM), cardiac sound separator, patient authentication and ECG coder. Various experiments showed that overall performance of all these ECG applications depends highly on accurate detection of time instants of the R-wave peaks in the ECG signal.[6,10,19,23,29] The typical ECG beat consists of P-wave, "QRS complex", T- and U-wave. The R-wave is the most prominent wave in each cardiac cycle of an ECG signal. Therefore, development of robust automatic R-wave peak detector is essential but it is still a challenging task due to irregular heart rates, various amplitude levels and shapes of QRS morphologies, and various kinds of noise and artifacts.

In the literature, many QRS detection methods have been developed based on the first and second derivatives, digital filters (DFs), linear prediction (LP), two-pole recursive filter, maximum a posteriori (MAP) estimation, wavelet transform (WT), filter-banks, Hilbert transform (HT), higher-order statistics (HOS), template matching (TM), geometrical matching (GM), matched filters, mathematical morphology, multiscale mathematical morphology (3M) and empirical mode

Address correspondence to M. Sabarimalai Manikandan, Department of Electronics and Communication Engineering, Amrita School of Engineering, Amrita Vishwa Vidyapeetham, Coimbatore 641105, India. Electronic mail: msm.sabari@gmail.com

decomposition (EMD), syntactical rules, neural networks, hidden Markov models (HMM), support vector machine (SVM), zero-crossing (ZC), and genetic algorithms.[1–9,12–16,18–20,22–28,30–32,34–38] Generally, the digital filtering based QRS detector is widely used because that has lower computational complexity, and requires less memory space.[20,25]

The QRS detectors based on filtering methods consists of two stages: the preprocessing stage and the decision stage.[25] The preprocessing stage is generally constructed using one or more signal processing techniques such as bandpass filters, derivatives filter banks, wavelets, EMD, mathematical morphological operators and squaring transformation. Although different signal processing techniques were employed to accentuate the QRS feature and to suppress the noises and artifacts but most of them have some drawbacks. Generally, nonlinear transformation plays an important role in detection performance. Therefore, the effectiveness of the traditional squaring transformation is studied using the ECG record 104 taken from the MIT-BIH arrhythmia database. The output results are illustrated in Fig. 1, which shows the original signal $x[n]$, the differentiated signal $d[n]$, the squared signal $e[n]$, and the feature signal $ee[n]$. It is noticed that the feature signal has more noise peaks and also the squarer buries the peaks of small-QRS and wide-QRS complexes under the high-amplitude ones. In such cases, many methods had a relatively high number of FN and FP detections for ECG signals with small-QRS and wide-QRS complexes and noise. Therefore, many researchers have attempted to construct suitable decision stage based on the preprocessing results for achieving better detection rates.

The decision stage generally includes peak-detection logic and searchback algorithm to locate R-peaks. The

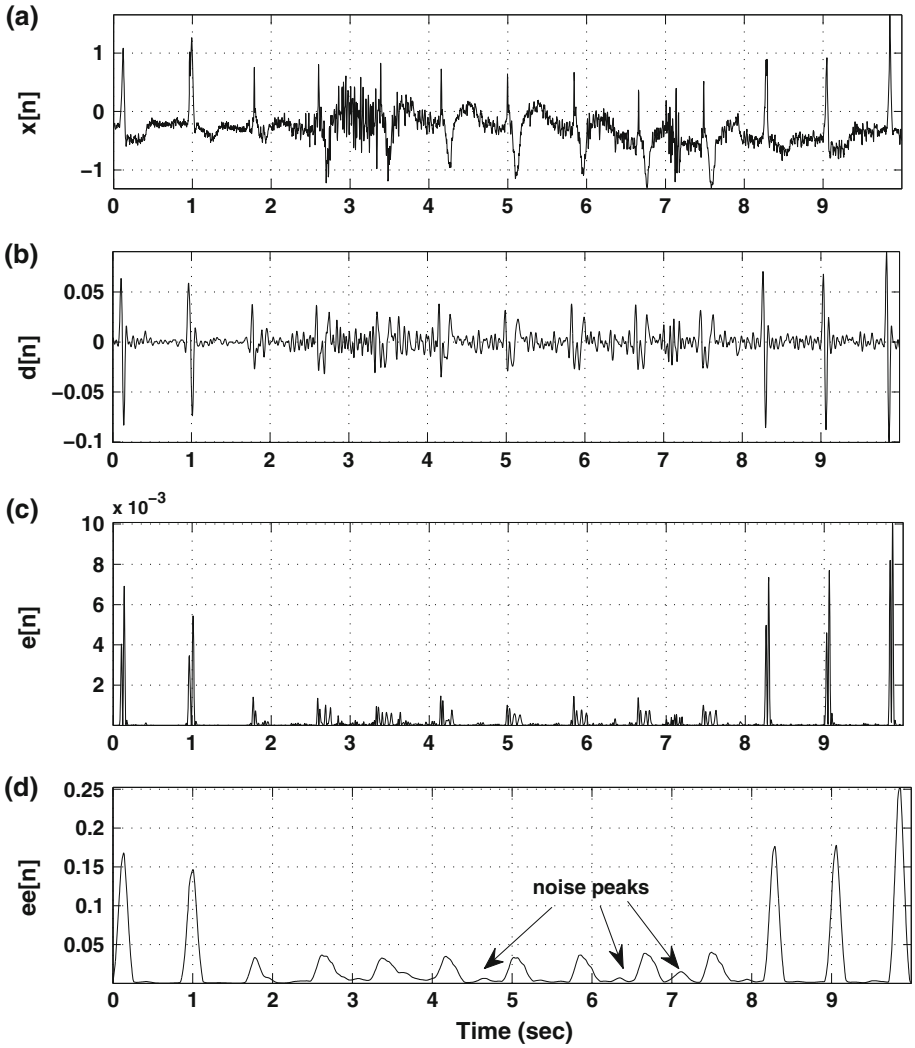

FIGURE 1. Example illustrating the output of stages of the conventional preprocessing algorithm. (a) Original ECG signal $x[n]$, (b) difference of the filtered ECG (dECG) signal $d[n]$, (c) squared (or energy) signal $e[n]$, and (d) energy envelope $ee[n]$.

decision stage of the filtering-based methods commonly consists of sets of heuristic decision rules and a set of tactics with fixed or/and adaptive amplitude-dependent, duration-dependent, and RR-interval-dependent thresholds for detecting R peaks in the feature signal.[4,14,20,26,30,35] These thresholds are updated periodically based upon amplitudes, durations and RR-intervals of detected R-peaks in the previous ECG segment. In literature, most of the algorithms use similar decision rules and threshold determination procedure. Moreover, searchback algorithm with adaptive amplitude-dependent and time-dependent thresholds were widely adopted to reject or include identified R-peaks located at t_m and t_n: (i) if $t_n - t_m < 0.2$ s (refractory period) and (ii) search back if $t_n - t_m > 1.5\mathrm{RR}_{\mathrm{avg}}$. These medical rules may improve detections for regular rhythms but some rules may be in conflict with others. The above detection issues clearly indicate that it is hard to find a proper set of decision rules and thresholds in case of (i) wide QRS complexes, (ii) low-amplitude QRS complexes, (iii) negative QRS polarities, (iv) sudden changes in RR intervals, (v) sudden changes in QRS amplitudes, (vi) sudden changes in QRS morphologies, (vii) sharp P/T waves, and various kinds of noise and artifacts.

In this paper, we present an effective and efficient automatic detection algorithm that identifies the time-location of the R-peaks in ECG signals. The proposed algorithm is simple that does not require additional decision rules with sets of thresholds based on the running estimates of the signal peaks and noise peaks, the average RR interval and rate limits, a set of tactics to reject or include identified R-peaks, and learning phase. The rest of this paper is organized as follows. "Proposed Algorithm Description and Theory" section describes a four-stage detection algorithm in detail, including pseudocode for implementation of the different stages. "Evaluation Methods" section describes the characteristics of validation ECG database, benchmark parameters, and the algorithm assessment procedure. "Results and Discussion" section reports the results of the proposed algorithm for the well-known MIT-BIH arrhythmia database and provides comparisons between the proposed algorithm and other existing algorithms. Finally, conclusions are drawn in last section.

PROPOSED ALGORITHM DESCRIPTION AND THEORY

In this section, we describe a simple and robust automated algorithm for detection of R-peaks of a long-term ECG signal. Figure 2 shows a block diagram of our R-peak detection algorithm that consists of the following steps:

- Bandpass Filtering and Differentiation
- New Nonlinear Transformation
- New Peak-Finding Technique
- Finding Location of True R-Peaks.

Bandpass Filtering and Differentiation

In the realistic environments, ECG signals are often obscured by various kinds of noise and artifacts from other sources. Common ECG noise sources such as power line interference, muscle contractions, baseline drift due to respiration, and abrupt baseline shift can corrupt ECG signals significantly. The frequency content of a QRS complex is essentially in the frequency range 5–30 Hz.[33] Heart pathologies may have a dramatic effect on the QRS complex. Several different choices of bandpass filters with different passband

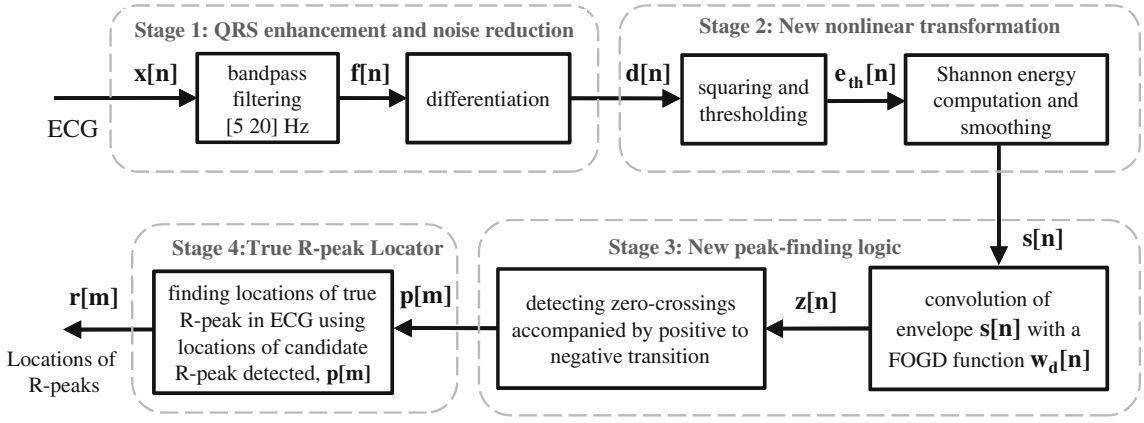

FIGURE 2. Block diagram showing the architecture and individual stages of the new detection algorithm for R-peak detection in ECG signals. A preprocessing stage emphasizes the QRS complex components and a new peak-finding stage identifies the location of candidate R-peak.

frequencies for enhancement of QRS complex and suppression of P/T waves and noises have been described.[25] Most of energies of noises generated by motion artifacts and P/T waves are concentrated up to 5 Hz. So, sufficient P/T wave and noise suppression up to 5 Hz is essential. Spectral analysis of the various QRS morphologies with duration between 0.05 and 0.2 s reveals that most of the frequencies present in the QRS complex lies below 20 Hz. In this work, we chose the passband such that they maximize the energy of different QRS complexes (narrow-QRS and wide-QRS complexes) and reduce the effect of P/T waves, power-line interference, motion artifacts and muscle noise. We construct the 15th-order FIR bandpass DF using the least squares approach, where cut-off frequencies of the passband are 6 and 20 Hz. After filtering, we apply first-order forward differentiation to emphasize large slope and high-frequency content of the QRS complex. Here, the differentiation of the filtered ECG signal $f[n]$ is implemented as

$$d[n] = f[n+1] - f[n]. \quad (1)$$

The derivative operation reduces the effect of large P/T waves. The original ECG and the difference of the filtered ECG (dECG) signals are shown in Figs. 3a and 3b, respectively. Figure 3b shows that the output of the

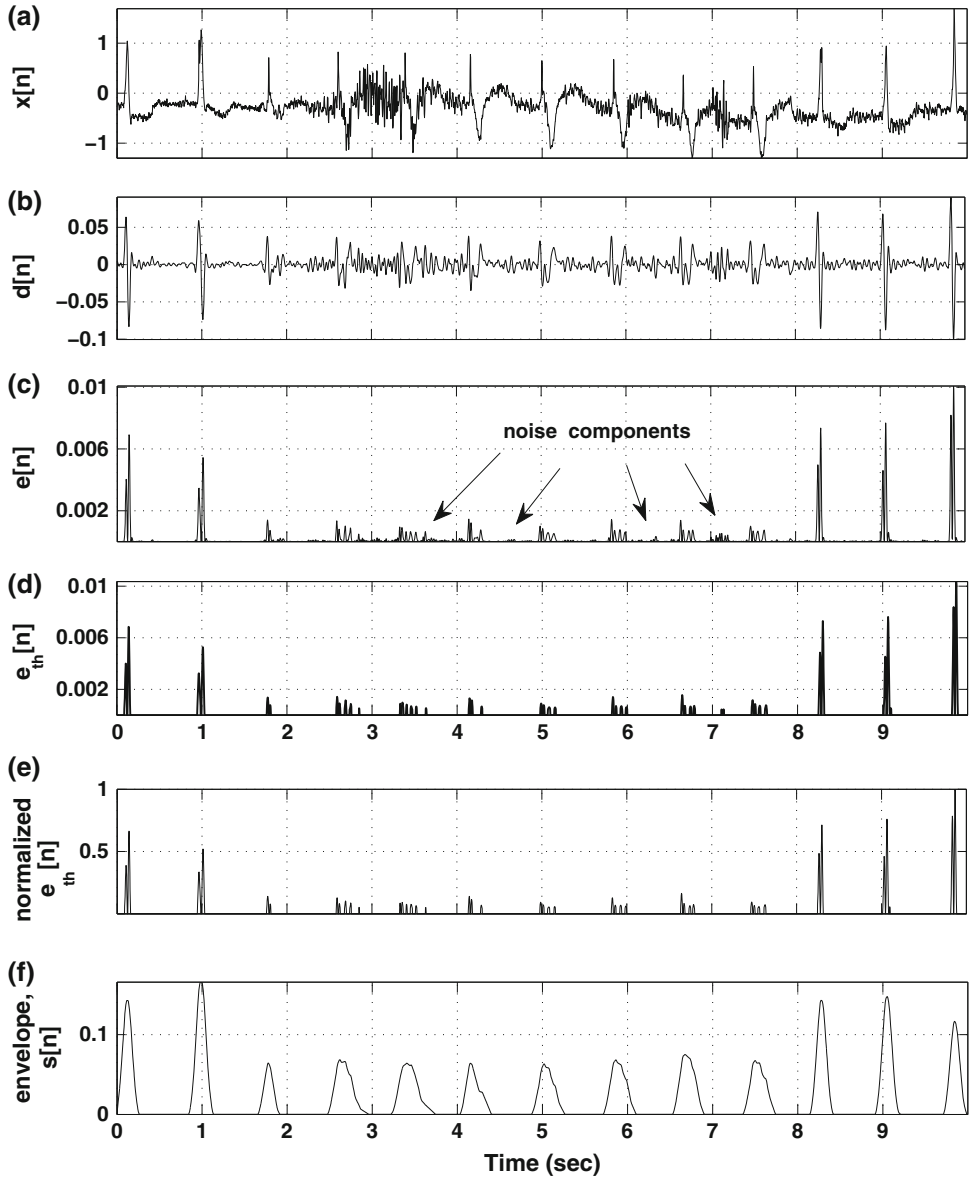

FIGURE 3. Example illustrating the output of stages of the proposed nonlinear transformation technique. (a) The original ECG signal $x[n]$, (b) the difference of the filtered ECG (dECG) signal $d[n]$, (c) the squared (or energy) signal $e[n]$, (d) the thresholded energy signal $e_{th}[n]$, (e) the normalized thresholded energy signal $\tilde{e}_{th}[n]$, and (f) the Shannon energy envelope $s[n]$.

differentiator is a bipolar signal. Thus, a rectification process (or nonlinear transformation) is employed to obtain a positive-valued signal that eliminates detection problems in case of negative QRS complexes. In literature, the squaring transformation is widely used to obtain positive peaks regardless of polarity of QRS complexes. Figure 1 illustrates that disadvantages of traditional squaring transformation: (i) it produces several spurious noise peaks and thus had a large number of false positives; and (ii) it buries the peaks of small-QRS and wide-QRS complexes under the high-amplitude ones. In such cases, most of the methods failed to detect smaller and wider-QRS complexes. Therefore, in this work, a new nonlinear transformation based on squaring, thresholding process and Shannon energy transformation is designed to combat such problems effectively.

New Nonlinear Transformation

Squaring and Adaptive Thresholding

The dECG signal $d[n]$ is first squared to obtain a positive-valued signal and then adaptive thresholding is performed on the energy (or squarer) values $e[n]$. The squaring is implemented as

$$e[n] = d^2[n]. \tag{2}$$

The thresholding function is defined as

$$e_{\text{th}}[n] = \begin{cases} 0, & e[n] < \eta \\ e[n], & \text{otherwise.} \end{cases} \tag{3}$$

In this thresholding process, the energy values $e[n]$ smaller than a threshold parameter η are set to zero and other values are retained. Here, the adaptive-threshold parameter η for each ECG segment is computed as

$$\eta = 0.5 \times \sigma_e, \tag{4}$$

where

$$\sigma_e = \sqrt{\frac{1}{N}\sum_{n=1}^{N}(e[n]-\mu)^2} \quad \text{and} \quad \mu = \frac{1}{N}\sum_{n=1}^{N} e[n]. \tag{5}$$

where N is the number of samples in a test ECG segment. The outputs of the squaring and thresholding stage is shown in Fig. 3. By comparing Figs. 3c and 3d, we can observe that the thresholding process effectively eliminates spurious noise spikes and tends to reduce the number of false positive detections under noisy ECG signal with long pauses.

Shannon Energy Computation and Smoothing

Since squarer buries the peaks of small-QRS and wide-QRS complexes under the high-amplitude ones, we thus use Shannon energy transformation which results in small deviations between the successive R peaks. The effectiveness of this nonlinear transformation was studied in our previous work.[30] The experimental results demonstrated that it improves detection accuracy under ECG signal with smaller- and wider-QRS complexes. To compute Shannon energy, the thresholded energy signal is first normalized as

$$\tilde{e}_{\text{th}}[n] = \frac{e_{\text{th}}[n]}{\max_{n=1}^{N}(|e_{\text{th}}[n]|)}, \tag{6}$$

and then the Shannon energy of the normalized signal $\tilde{e}_{\text{th}}[n]$ is computed as

$$s[n] = -\tilde{e}_{\text{th}}^2[n]\log\tilde{e}_{\text{th}}^2[n]. \tag{7}$$

The Shannon energy values are smoothed using the finite-impulse response (FIR) filter with a rectangular impulse response $h[k]$ of length L to reduce the effect of multiple peaks around QRS complex regions. This smoothing process is designed to generate peaks corresponding to the QRS-complex portions. The proposed nonlinear transformation generates a smooth feature signal that is illustrated in Fig. 3f. We can clearly notice that the locations of candidate R-peaks in the SE envelope $s[n]$ correspond to approximate locations of the R peaks in the ECG waveform shown in Fig. 3a. Therefore, in this proposed algorithm, these candidate peaks are processed further to find locations of true R peaks in a ECG signal.

New Peak-Finding Logic Using the First-Order Gaussian Differentiator

This section describes a new and simple peak-finding strategy using the first-order Gaussian differentiator (FOGD) operator that automatically finds the locations of candidate R-peaks in the SE envelope.

The First-Order Gaussian Differentiator

In this work, the M-point Gaussian window $w[m]$ is defined as

$$w[m] = e^{-\frac{1}{2}\frac{\left(m-\frac{M}{2}\right)^2}{\sigma^2}}, \quad m = 1, 2, 3, \ldots, M \tag{8}$$

and the FOGD is computed as

$$w_{\text{d}}[m] = w[m+1] - w[m], \quad m = 1, 2, 3, \ldots, M-1 \tag{9}$$

which gives the slope at each sample. The 901-point Gaussian window with spread $\sigma = 36$ is shown in Fig. 4a and the corresponding FOGD function is shown in Fig. 4b. We can observe that the Gaussian window is symmetric about $\lfloor\frac{M}{2}\rfloor + 1$ and its first-order

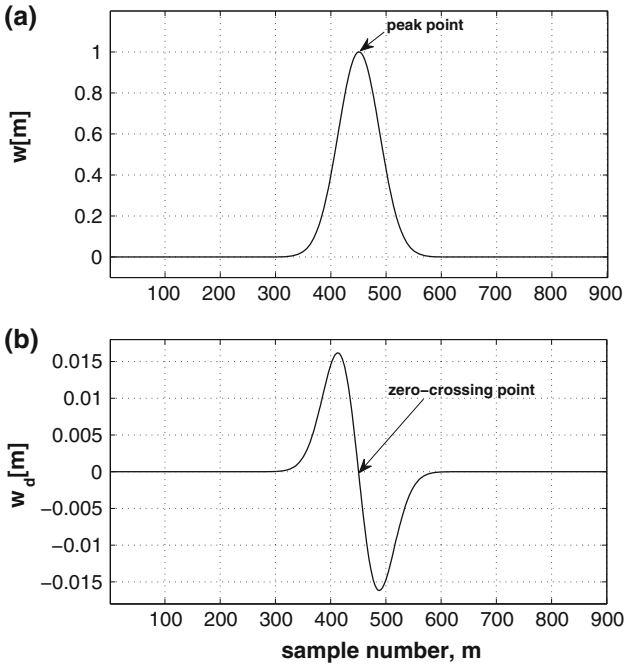

FIGURE 4. (a) The 901-point Gaussian window with spread σ = 36 and (b) the FOGD $w_d[m]$.

derivative is an antisymmetric function. Figure 4a shows that the Gaussian window function has a peak at $m = \lfloor \frac{M}{2} \rfloor + 1$. Figure 4b shows that the slope of FOGD is positive and negative for $1 \leq m \leq \lfloor \frac{M}{2} \rfloor$ and $\lfloor \frac{M}{2} \rfloor + 1 \leq m \leq M$, respectively and also its slope is zero at $m = \frac{M}{2}$, where $\lfloor \cdot \rfloor$ denotes the floor function. This is the basis for the proposed peak-finding logic. For detecting candidate R-peaks in SE envelope, we perform the convolution operation on the SE envelope $s[n]$ and the FOGD sequence $w_d[m]$ that is computed as

$$z[n] = \sum_{k=-\infty}^{\infty} w_d[k]\, s[n-k]. \tag{10}$$

The convolution output of the FOGD function $w_d[m]$ with a Shannon energy envelope $s[n]$ is shown in Fig. 5c. In this work, the convolution output is referred to as ZC function $z[n]$ that has both positive and negative ZCs because of the anti-symmetric nature of the FOGD function.[27] Positive ZC is defined as a ZC associated with a positive slope that can be obtained if the signal moves from a negative to a positive value. If the signal $z[n]$ moves from a positive to a negative value, it is a negative ZC, which has a negative slope. Figure 5c demonstrate that negative ZCs indicate locations of the peaks in the Shannon energy envelope $s[n]$ shown in Fig. 5b. Therefore, negative ZCs are detected and used as guides to find locations of R-peaks in the original ECG signal shown in Fig. 5a.

Detecting Negative Zero-crossings

In this work, negative ZCs are detected by checking the sign of the ZC function $z[n]$ at time instants t_n and t_{n+1}. The pseudocode for this function is shown in Table 1 and its output is illustrated in Fig. 5d. By comparing Figs. 5d and 5b, it can be observed that the proposed peak-finding technique accurately identifies time locations of candidate R-peaks in the SE envelope. The output shown in Fig. 5e illustrates that the detected time instants are slightly shifted from the instants of real R peaks in the ECG signal. Therefore, in the next stage, the detected time instants of candidate R-peaks are used as guides to locate real R-peaks.

Finding Location of Real R-Peaks

To find time instants of real R-peaks in an original ECG signal, this stage uses locations of all candidate R-peaks detected at the previous stage. First, a segment centered around each location of detected candidate R-peak $(p[m] \pm \frac{K}{2})$ is extracted from the original ECG signal. Then, a simple algorithm finds the location of maximum peak value in the segment. This process is repeated for all the detected locations $p[m]$. Table 2 list the pseudocode for this function. The output of this stage is shown in Fig. 5f. The results show that the locations of real R-peaks are accurately detected regardless of varying amplitudes and shapes of QRS complexes and noise.

EVALUATION METHODS

Characteristics of Validation Database

Many of the existing algorithms were not evaluated against a standard database and also not measured the detection performance using the benchmark parameters.[20] This makes the experimental results difficult to compare and to assess. Therefore, we evaluate the performance of the proposed algorithm using the well-known MIT-BIH arrhythmia database. It contains 48 half-hour of two-channel ECG recordings sampled at 360 Hz with 11-bit resolution over a 10 mV range. The ECG records from this database include signals with acceptable quality, sharp and tall P and T waves, negative QRS complex, small QRS complex, wider QRS complex, muscle noise, baseline drift, sudden changes in QRS amplitudes, sudden changes in QRS morphology, multiform premature ventricular contractions (PVCs), long pauses and irregular heart rhythms. In this study, we consider the entire ECG recordings since the proposed algorithm does not require any learning phase. Episodes of ventricular flut-

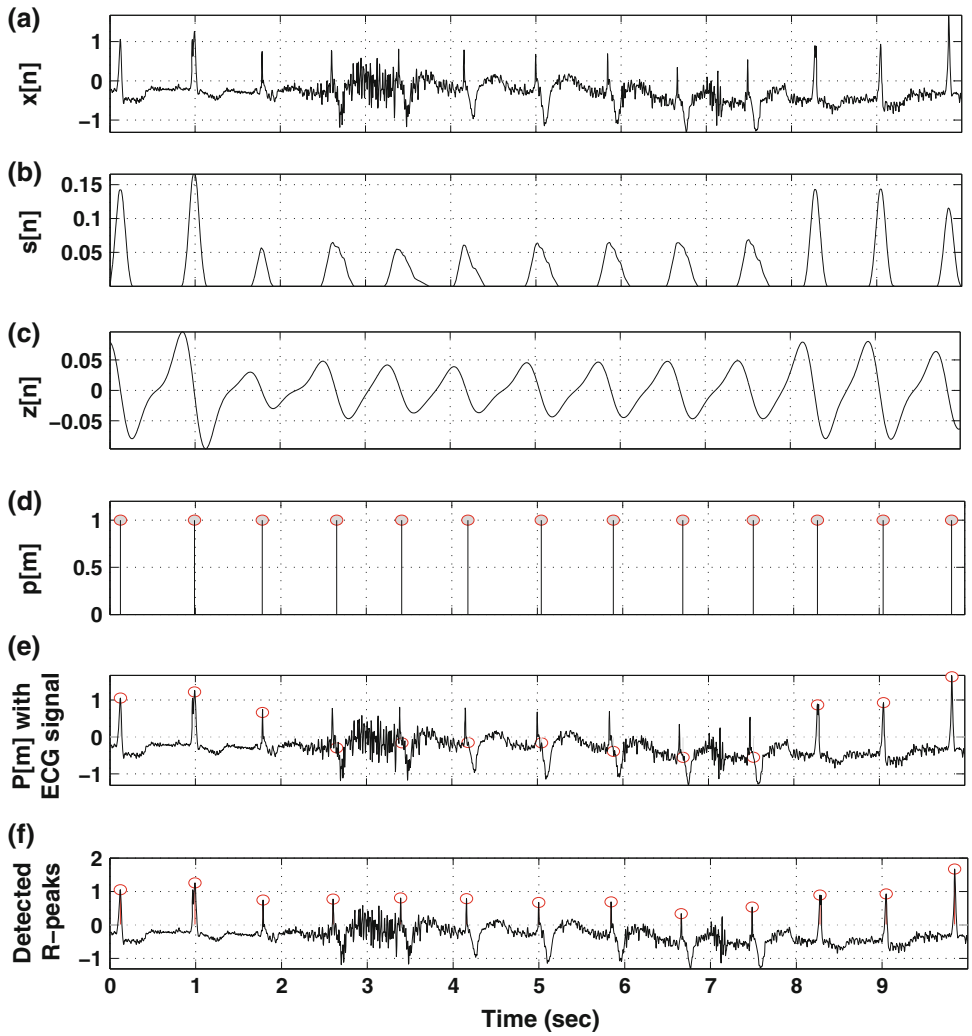

FIGURE 5. Example illustrating the output of stages of the proposed nonlinear transformation and peak-finding logic techniques. (a) The original ECG signal $x[n]$, (b) the Shannon energy envelope $s[n]$, (c) the convolution output of SE envelope $s[n]$ with the FOGD function $w_d[m]$, (d) the time instants of negative ZCs that correspond to locations of peaks in the SE $s[n]$, (e) detected time instants of candidate R-peaks with the original ECG signal, and (f) detected time-instants of real R-peaks in the ECG signal.

TABLE 1. Algorithm pseudocode: DetectNegativeZerocrossing.

Function: p=DetectNegativeZerocrossing
Inputs
z:= Input signal. Here, input signal is a convolution output, $z[n]$.
N:= Size of signal (in samples).
Outputs
p:=Locations of negative ZCs.
Begin
Initialize $k = 1$.
for $n = 1$ to $N - 1$, increment by 1,
  if (sign($z[n]$) > 0) & & (sign($z[n + 1]$) < 0),
  p[**k**] := n // storing location of negative ZC.
 end.
End.

ter in ECG record 207 are excluded from the performance analysis for better comparison with the other detection methods.[4,23]

Algorithm Implementation and Assessment

The proposed algorithm is implemented in MATLAB on a 2.4-GHz Intel core 2 Quad CPU. The algorithm is tested on the ECG signals taken from the first channel of the MIT-BIH arrhythmia database. The choice of smoothing filter length (L) and the Gaussian window length (M) is very important that may affect the detection performance. The larger value of M may merge two consecutive R-peaks in the ECG signal. In this work, the average of lower and upper limits of QRS complex duration is considered to determine the length of the smoothing filter. The duration of normal QRS and wide QRS complexes is usually between 0.05 and 0.2 s. For the sampling rate of 360 samples per second, the length of the smoothing filter is 0.125 times the sampling rate. By considering

TABLE 2. Algorithm pseudocode: FindingRealRpeaks.

Function: r=FindingRealRpeaks
Inputs
$y[n]$:= Filtered ECG signal; $n = 1, 2, 3, \ldots N$
$p[m]$:=Locations of detected candidate R-peaks; $m = 1, 2, 3 \ldots M$.
M:= Total number of detected peaks.
K:=window size.
Outputs
$r[m]$:=Locations of real R-peaks in ECG signal.
Begin
if $p[1] < \frac{K}{2}$
  $p[m] := p[m] + \frac{K}{2}, m = 1, 2, 3 \ldots M$.
  zpd:=zeros$(1, \frac{K}{2})$,
  $y[1 \text{ to } (\text{length}(x) + \frac{K}{2})] := [\text{zpd } x]$; zero-padding process.
else $(p[M] + \frac{K}{2}) < N$
  zpd:=zeros$(1, \frac{K}{2})$,
  $y[1 \text{ to } (\text{length}(x) + \frac{K}{2})] := [x \text{ zpd}]$; zero-padding process.
end,
for $m = 1$ to M, increment by 1,
  SegStartPosition $:= p[m] - \frac{K}{2}$,
  SegEndPosition $:= p[m] + \frac{K}{2}$,
  ECGSeg $:= y$[SegStartPosition to SegEndPosition],
  [maxvalue maxindex] $:= \max_k^K(|\text{ECGSeg[k]}|)$,
  r[**m**] := maxindex + SegStartPosition,
End.

the upper limits of heart rates in practice, the Gaussian window length (L) is computed as 2.5 times the sampling rate. In this study, the smoothing filter length (L) and the Gaussian window length (M) of the detector are set as (L, M) = (45,900) samples.

The performance of the algorithm is validated by comparing the results of automatic annotations against cardiologist annotations. The basis of standard clinical electrocardiography is the 10-s 12-lead ECG.[11,17,21] The usual duration of computer evaluated ECG records is 10-s, which typically contain a number of heartbeats and hence a number of diagnostic parameters such as amplitude, duration, interval, and shape of the ECG beat. In many ECG signal analysis, the first stage is to locate the peaks of the QRS complexes in the 10-s ECG signal. In data compression for transmission, storage, and retrieval of ECGs, 10 s of an ECG signal is considered. Therefore, in this work, each ECG record is divided into ECG segments with duration of 10-s. Then, each ECG segment is processed and the detected R-peaks are verified by visual inspection. While performing the visual inspection on the automatic annotation results, we calculate three quantities: (i) true-positive (TP) when a R-peak is correctly detected by the proposed algorithm; (ii) false-negative (FN) when a R-peak is missed; and (iii) false-positive (FP) when a noise spike is detected as R-peak. Based on the previous works in the field of computer-aided ECG signal analysis,[6,10,19,23] we therefore process an ECG segment with duration of 10-s. The average time required to process 10-s ECG segment is 6.4-ms.

Benchmark Parameters

In this work, we adopt the following the benchmark parameters reported by the Association for the Advancement of Medical Instrumentation (AAMI): sensitivity (Se) and positive predictivity ($+P$) to assess the performance of the proposed algorithm. The Se indicates the percentage of correctly detected true R-peaks by the algorithm to total number of R-peaks of original ECG signal. The $+P$ indicates the percentage of correctly detected true R-peaks to total number of peaks marked by the algorithm. The sensitivity, positive predictivity and the detection error rate (DER) are computed as

$$Se = \frac{TP}{TP + FN} \times 100\%, \tag{11}$$

$$+P = \frac{TP}{TP + FP} \times 100\%, \tag{12}$$

$$DER = \frac{FP + FN}{TP} \times 100\%. \tag{13}$$

The overall performance is measured in terms of a detection accuracy, which is computed as

$$\text{Accuracy (Acc)} = \frac{TP}{TP + FP + FN} \times 100\%. \tag{14}$$

RESULTS AND DISCUSSION

In this section, we report the experimental results and provide comparisons between proposed algorithm and other existing algorithms. Table 3 summarizes sensitivity and positive predictivity of the proposed algorithm for test ECG signal taken from first-channel (each) of 48 ECG recordings of the MIT-BIH arrhythmia database. The proposed algorithm produces 76 false-negative (FN) beats and 38 false-positive (FP) beats for a total detection failure of 114 beats. But the individual detection accuracies for ECG records vary from 99.21 to 100% depending on the characteristics of normal and pathological ECG signals, and different noises.

The different stages and the overall performance of nine R-peak detection algorithms are summarized in Table 4. The proposed algorithm achieves an average accuracy of 99.90%, a sensitivity of 99.94%, and a positive predictivity of 99.96% are obtained against the first-channel of the ECG recordings of the MIT-BIH arrhythmia database. The proposed algorithm achieved better performance than the other detection algorithms reported in Table 4.

TABLE 3. Performance of the proposed algorithm with the MIT-BIH arrythmia database (detection parameters: smoothing filter length (*L*) and Gaussian window length (*L*)), (*M*, *L*) = (45,900) samples).

ECG record	Total (beats)	FN (beats)	FP (beats)	DER (%)	Se (%)	+*P* (%)	Accuracy (%)
100	2273	0	0	0	100	100	100
101	1865	0	0	0	100	100	100
102	2187	0	0	0	100	100	100
103	2084	0	0	0	100	100	100
104	2229	0	9	0.404	100	99.60	99.60
105	2572	3	8	0.428	99.88	99.69	99.57
106	2027	4	0	0.197	99.80	100	99.80
107	2137	0	0	0	100	100	100
108	1763	1	4	0.284	99.94	99.77	99.72
109	2532	0	0	0	100	100	100
111	2124	0	0	0	100	100	100
112	2539	0	0	0	100	100	100
113	1795	0	0	0	100	100	100
114	1879	0	1	0.053	100	99.95	99.95
115	1953	0	0	0	100	100	100
116	2412	18	1	0.788	99.25	99.96	99.21
117	1535	0	0	0	100	100	100
118	2278	0	0	0	100	100	100
119	1987	0	0	0	100	100	100
121	1863	0	0	0	100	100	100
122	2476	0	0	0	100	100	100
123	1518	0	0	0	100	100	100
124	1619	0	0	0	100	100	100
200	2601	0	0	0	100	100	100
201	1963	1	0	0.051	99.95	100	99.95
202	2136	1	0	0.047	99.95	100	99.95
203	2980	14	2	0.537	99.53	99.93	99.46
205	2656	3	0	0.113	99.89	100	99.89
207	1862	0	0	0	100	100	100
208	2955	15	0	0.508	99.49	100	99.49
209	3005	0	0	0	100	100	100
210	2650	11	0	0.415	99.58	100	99.58
212	2748	0	0	0	100	100	100
213	3251	0	0	0	100	100	100
214	2262	0	1	0.044	100	99.96	99.96
215	3363	0	0	0.000	100	100	100
217	2208	2	0	0.091	99.91	100	99.91
219	2154	0	0	0	100	100	100
220	2048	0	0	0	100	100	100
221	2427	0	0	0	100	100	100
222	2483	0	0	0	100	100	100
223	2605	0	0	0	100	100	100
228	2053	2	10	0.585	99.90	99.51	99.42
230	2256	0	0	0	100	100	100
231	1571	0	0	0	100	100	100
232	1780	0	2	0.112	100	99.89	99.89
233	3079	1	0	0.032	99.97	100	99.97
234	2753	0	0	0	100	100	100
Overall	109,496	76	38	0.098	99.94	99.96	99.90

Detection parameters: smoothing filter length (*L*) and Gaussian window length (*L*), (*M*, *L*) =(45,900) samples.

The MIT-BIH arrhythmia database ECG recordings 104, 105, 106, 108, 113, 116, 200, 201, 202, 203, 208, 209, 210, 221, 222, 223, 228, 231, and 232 often create more detection errors with other algorithms, but significant improvement is achieved with our algorithm. The ECG records 104, 105, 108, 200, 203, 210, and 228 contain high-grade noise and artefact. Records 108, 111, 112, 116, 201, 203, 205, 208, 210, 217, 219, 222, and 228 include severe baseline drifts and abrupt changes in QRS morphology. Records 201, 202, 203, 219 and 222 exhibits various irregular rhythmic patterns. Records 201, 219 and 232 include long pauses up to 6 s in duration. Records 108 and 222 contain large sharp P waves. Records 111, 113, and 117 contain large T waves. For these ECG recordings, most algorithms produced a large amounts of false positives. Records 200, 203 and 233 contain multiform ventricular arrhythmia, negative QRS polarity and sudden changes in QRS morphology. Record 208 has wider PVCs. Record 223 exhibits sudden changes in QRS amplitudes. Records 116 and 208 contain smaller QRS complexes than the others. For these ECG recordings, most of the algorithms had higher false-negative detections.

The effectiveness of the proposed algorithm in terms of the number of false negatives and false positives is shown in Table 5. The DF-based algorithm[14] and the EMD-based algorithm[15] produced a total detection failure of 530 beats (325 FP beats and 205 FN beats), and of 506 beats (209 FP and 297 FN beats), respectively. Recently, it has been shown that the multiscale mathematical morphology (3M) filtering based algorithm[36] and the mathematical morphology and wavelet transform (MMWT) based algorithm[37] achieve the lowest total DER and outstanding false positive and false negative rates. Thus, it is necessary to compare the performance of these algorithms. For the high-grade noise and artifacts (Record 105), the 3M filtering- and MMWT-based algorithms had DERs of 1.01% (26 beats) and 1.67% (43 beats), respectively whereas the proposed algorithm produces 8 FP beats (0.311%) and 3 FN beats (0.117%) for a DER of 0.428% (11 beats). In the case of the very big changes in shape of QRS complex and amplitude of QRS complex (record 106 shown in Fig. 7), our algorithm shows a detection failure rate of 0.197% (4 beats). For this record, the 3M filtering-based algorithm and the MMWT-based algorithm showed total detection failure of 2.02% (41 beats) and of 1.68% (34 beats), respectively. The numerous long pauses up to 6 s in duration are mainly found in record 232 that yields more false positive detections in most of the algorithms. To test the robustness of our algorithm, the non-stationary noise is added to the ECG signal. The detection results of our algorithm for the ECG signal with RR-interval greater than 4-s are shown in Fig. 11. The comparison result of 30-min record 232 in Table 5 demonstrates that the proposed algorithm produces two false positive beats and achieves outstanding false

TABLE 4. Preprocessing and decision stages of R-peak detection algorithms and comparison of their overall detection performance.

	Methodology								
Ref.	Preprocessing stage	Primary threshold, θ_{pt}	Secondary threshold, θ_{st}	Blanking	FP (beats)	FN (beats)	Se (%)	P^+ (%)	Acc (%)
[14]	Bandpass filtering → derivative → squaring → moving-window integration → feature signal $s[n]$	θ_{pt} = threshold coefficient × median of eight past peak levels	$\theta_{st} = 0.3 \times \theta_{pt}$ if RR > 1.5 × median of past RR intervals	Refractory period of 0.2 s, T-wave removal	248	340	99.69	99.77	99.46
[4]	Bandpass filtering → derivative → squaring transformation → feature signal $s[n]$	Finding the threshold of segment i: $\theta_{pt}^{(i)} = 0.39M_i$, if $\mathrm{RMS}_i > 0.18\ M_i$ && $M_i \le 2M_{i-1}$ $= 0.39\ M_{i-1}$, if $\mathrm{RMS}_i > 0.18\ M_i$ && $M_i > 2M_{i-1}$ $= 1.6\mathrm{RMS}_i$, if $\mathrm{RMS}_i < 0.18\ M_i$	$\theta_{st} = 0.5 \times \theta_{pt}$	T-wave removal 0.2–0.36 s	447	467	99.57	99.59	99.17
[23]	Quadratic spline wavelet decomposition, four scales	Four thresholds for QRS detection: $\epsilon_{qrs}^{i} = \mathrm{RMS}(W_{2^i}x[n]), \quad i = 1, 2, 3$ $\epsilon_{qrs}^{4} = 0.5\mathrm{RMS}(W_{2^4}x[n])$ Thresholds to check significance: $\gamma_{qrs_{pre}} = 0.06\max(\lvert W_{2^2}x[n]\rvert)$, $\gamma_{qrs_{post}} = 0.09\max(\lvert W_{2^2}x[n]\rvert)$,	Searchback with lowered thresholds	Refractory period of 0.2 s	153	220	99.80	99.86	99.66
[15]	EMD → soft-thresholding rule → constructing the layer: the detection layer, the verification layer, the leakage layer → feature signal $s[n]$	Four thresholds: window size (W) $\varepsilon^{(d)} = 0.3(0.7M_i^{(d)} + 0.3A^{(d)})$ $\theta_1^{(ld)} = 0.25(A_i^{(ld)} + A_{i+1}^{(ld)})$, W=10-ms $\theta_2^{(ld)} = 0.375(A_i^{(ld)} + A_{i+1}^{(ld)})$, W=20-ms $\theta_3^{(ld)} = 0.6A_i^{(ld)}$, W=30-ms where M^d is the highest value of the modulus maxima in i^{th} segment, A^d is the average value of the R-wave amplitudes in d layer, A^{ld} & A^{ld} are the two R-wave amplitudes in $(i-1)^{th}$ segment within that leakage period in ld layer.	$\theta_{st} = 0.5 \times \theta_{pt}$	Refractory period of 300 ms	467	244	99.77	99.56	99.33
[3]	Bandpass filtering (four filters) → derivative → squaring → feature signal $s[n]$ → computing positive average slope and negative average slope for each five consecutive samples	Automatic thresholds calculation: $\mathrm{THV}_p[m] = \alpha(\frac{1}{5}\sum_{l=m-4}^{m} \mathrm{S}_p[l])$ $\mathrm{THV}_n[m] = \beta(\frac{1}{5}\sum_{l=m-4}^{m} \mathrm{S}_n[l])$ $\mathrm{THV}_a[m] = \gamma(\frac{1}{5}\sum_{l=m-4}^{m} \mathrm{P}_a[l])$ S_p = positive slope; S_n = negative slope; P_a = peak amplitude; α, β, and γ are the coefficients that are found empirically	Search back with adaptive thresholds	<263 ms	393	253	99.77	99.64	99.41
[9]	Baseline drift & noise removal → apply coiflet wavelet → squaring → moving averaging → feature signal $s[n]$	Threshold based on the SNR computed between wavelet coefficients at 1st & 5th level coefficients at 1st & 5th level	None	None	214	1333	99.78	99.80	98.59

TABLE 4. Continued.

Ref.	Methodology					FP (beats)	FN (beats)	Se (%)	P^+ (%)	Acc (%)
	Preprocessing stage	Primary threshold, θ_{pt}	Secondary threshold, θ_{st}	Blanking						
36	Three morphology filtering → derivative → absolute of $v[n]$ → multiple-frame accumulation → feature signal $s[n]$	$\theta_{pt} = 0.1\text{Max}_i$, $\text{Max}_i < 3$ $= 0.27\text{Max}_i$, $3 \le \text{Max}_i \le 5$ $= 0.15\text{Max}_i$, $\text{Max}_i > 5$ Max_i = maximum value of i^{th} segment	None	None		204	213	99.81	99.80	99.62
30	Bandpass filtering → derivative → normalization → Shannon energy → smoothing → feature signal $s[n]$	HT of $s[n] \rightarrow$ LF drift removal → negative ZCs detection → real R-peaks detection → output:time instants of R-peaks	None	None		140	79	99.93	99.88	99.80
Our work	Bandpass filtering → derivative → squaring → thresholding → normalization → Shannon energy & smoothing → feature signal $s[n]$	Convolution of $s[n]$ with $w_d[n] \rightarrow$ negative ZCs detection → real R-peaks detection → output: time instants of R-peaks	None	None		38	76	99.94	99.96	99.90

positive values compared to recently reported algorithms.

Many algorithms have large number of false-negative (or missed detections in case of ECG signals with abrupt change in amplitude of QRS complex, small QRS complex, and wide QRS complex. To detect missed R-peaks, almost all algorithms used sets of heuristic decision rules with adaptive amplitude, RR-interval and duration thresholds estimated for the previous detected R-peaks. It was seen that the algorithm with secondary threshold produces several spurious peaks. Thus, the refractory period of 200 ms and T-wave discriminator (200–360 ms) are widely used in most of the algorithms. It can been seen that the ECG record 203 has many shortest RR-intervals of less than 360 ms. These decision rules with amplitude-dependent threshold may yield the poorest results in the case of ECG signal with irregular heart rhythm, continuously varying QRS morphology, and noise and artifacts. Furthermore, the performance of many algorithms highly rely on an accurate measurement of initial parameters in the learning phase. The performance comparison in Table 5 shows that the proposed algorithm has a total detection failure of 106 beats (36 FP beats and 70 FN beats) and outperforms the other algorithms reported in Adnane *et al.*,[3] Darrington,[8] Elgendi *et al.*,[9] Hamilton and Tompkins,[14] Hongyan and Minsong,[15] and Zhang and Lian.[36,37] In this work, the proposed algorithm does not use additional decision rules with sets of thresholds based on the running estimates of the signal peaks and noise peaks, the average RR interval and rate limits, a set of rules for blanking and T-wave discrimination, and training phase.

The waveforms of the different stages of the proposed algorithm using the ECG segments taken from first-channel of the different recordings of the MIT-BIH arrhythmia database are shown in Figs. 6–12. In each of these figures, waveform depicted in (a) is the original ECG signal, $x[n]$. The waveform depicted in (b) is the differenced bandpass filtered signal, $d[n]$. The waveform (c) is the smooth Shannon energy envelogram (SEE) of the thresholded signal $\tilde{e}_{th}[n]$. The SEE is used as the feature signal. The waveform (d) is the convolution of the feature signal $s[n]$ with FOGD function $w_d[n]$. The waveform depicted in (e) shows the time instants (marked in red circle) of detected R-peaks using the proposed algorithm. In our previous work in Sabarimalai Manikandan and Dandapat,[30] the decision stage includes HT, moving average (MA) filter and ZC detector. In this proposed algorithm, the decision stage includes two steps: (i) the convolution of the FOGD function $w_d[m]$ with the Shannon energy envelope $s[n]$, and (ii) the negative ZCs detection. Experiments show that the proposed FOGD-based

TABLE 5. Comparison of numbers of false-positives and false-negatives for pathological and noisy records of the MIT/BIH database.

		Number of false-positive (FP) detections								Number of false-negative (FN) detections							
Rec. No.	ECG signal quality	DF[14]	EMD[15]	WT[9]	3MM[36]	Slope[3]	Maxima[8]	MMWT[37]	Our	DF[14]	EMD[15]	WT[9]	3MM[36]	Slope[3]	Maxima[8]	MMWT[37]	Our
104	Multiform PVCs & severe muscle noise	3	20	0	7	63	25	13	9	7	1	0	1	12	25	2	0
105	High-grade noise and artifacts	53	35	15	7	28	51	38	8	22	14	21	19	6	28	5	3
106	Abrupt changes in QRS morphology	1	5	0	21	02	28	10	0	2	0	0	20	17	9	24	4
108	Sharp-tall P-wave, negative QRS complexes, & severe noise and artifacts	50	68	2	10	55	178	14	4	47	9	62	2	28	48	2	1
113	Sharp-tall T-wave & baseline drifts	2	6	1	10	0	0	5	0	1	0	682	11	1	9	5	0
116	Very small QRS (Amp. <0.05 mV)	4	–	20	4	3	1	0	1	25	–	0	27	20	28	21	18
200	Multiform PVCs with noise and artifact	3	47	1	4	47	122	0	0	2	3	2	9	0	102	2	0
201	Junctional escape beats	3	3	1	2	0	0	0	0	19	10	66	4	3	21	10	1
202	Irregular heart rates and low-QRS	0	5	1	2	0	1	0	0	3	6	3	6	2	9	17	1
203	Very big change in adjacent QRS-shape, QRS-amplitude, heart rates, very small QRS (<0.04 mV), noise & artifacts	14	23	79	3	27	88	2	2	61	95	19	7	53	45	23	14
208	Wide-QRS & small-QRS <0.05 mV	9	2	13	3	5	18	1	0	19	19	3	10	30	39	9	15
209	Bursts of noise	2	0	0	2	1	29	2	0	2	0	1	9	0	17	12	0
210	Small QRS complexes, noise & artifacts	2	8	5	16	8	10	11	0	41	23	2	5	29	54	1	11
221	Wide QRS complexes	1	4	0	4	0	16	0	0	1	2	4	8	4	12	3	0
222	Irregular heart rates & small QRS	40	5	27	1	3	3	1	0	37	0	12	0	0	13	6	0
223	Abrupt change in amplitude of R-peak	0	28	0	4	0	4	6	0	2	1	0	22	1	12	1	2
228	Severe noise & very big change in amplitudes of adjacent R-peaks	19	38	1	10	76	14	20	10	6	22	14	2	6	15	8	0
231	Irregular heart rates	0	2	0	7	0	0	22	0	0	0	331	1	0	9	5	0
232	Numerous long pauses up to 6 s	3	26	0	14	20	31	29	2	0	0	17	2	0	8	5	0
Total		209	325	166	131	338	619	174	36	297	205	1239	165	212	503	161	70

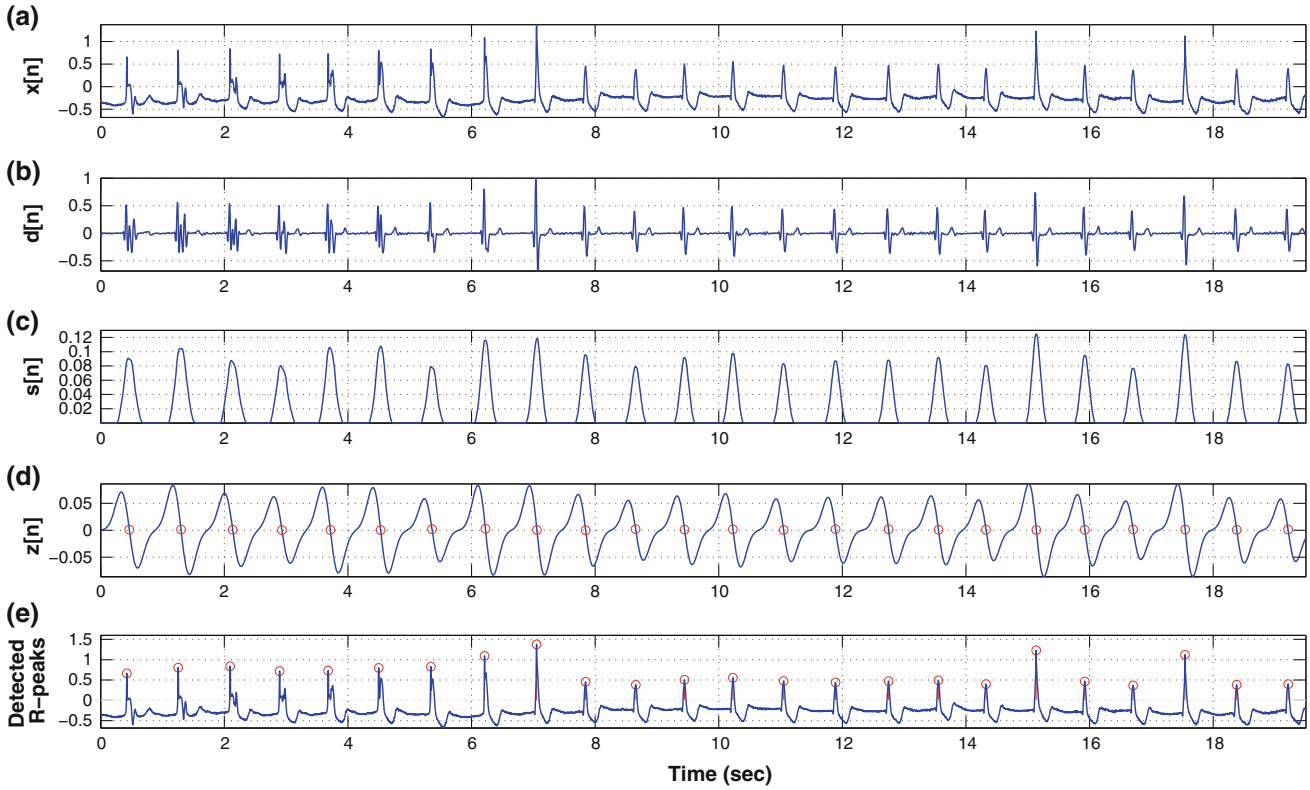

FIGURE 6. Performance of the proposed algorithm for ECG record 102 with varying QRS complex morphologies. Our algorithm produces 0 missed beats and 0 FP beats for a total of 2187 true beats. Detection accuracy is 100%.

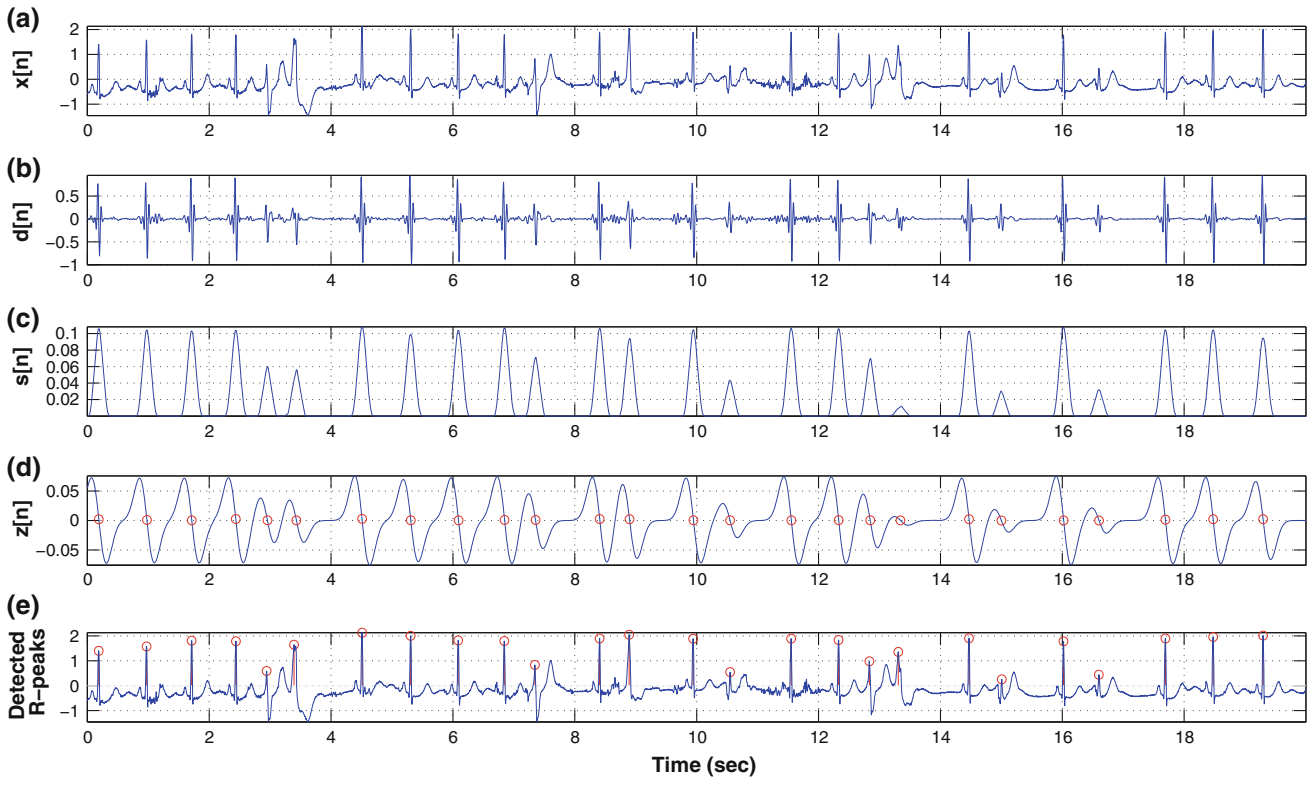

FIGURE 7. Detection performance for the ECG signal with continuously varying QRS complex morphology, sudden changes in beat-to-beat RR-interval, and tall T waves (Record 106). Our algorithm produces 04 missed beats and 0 FP beats for a total of 2027 true beats.

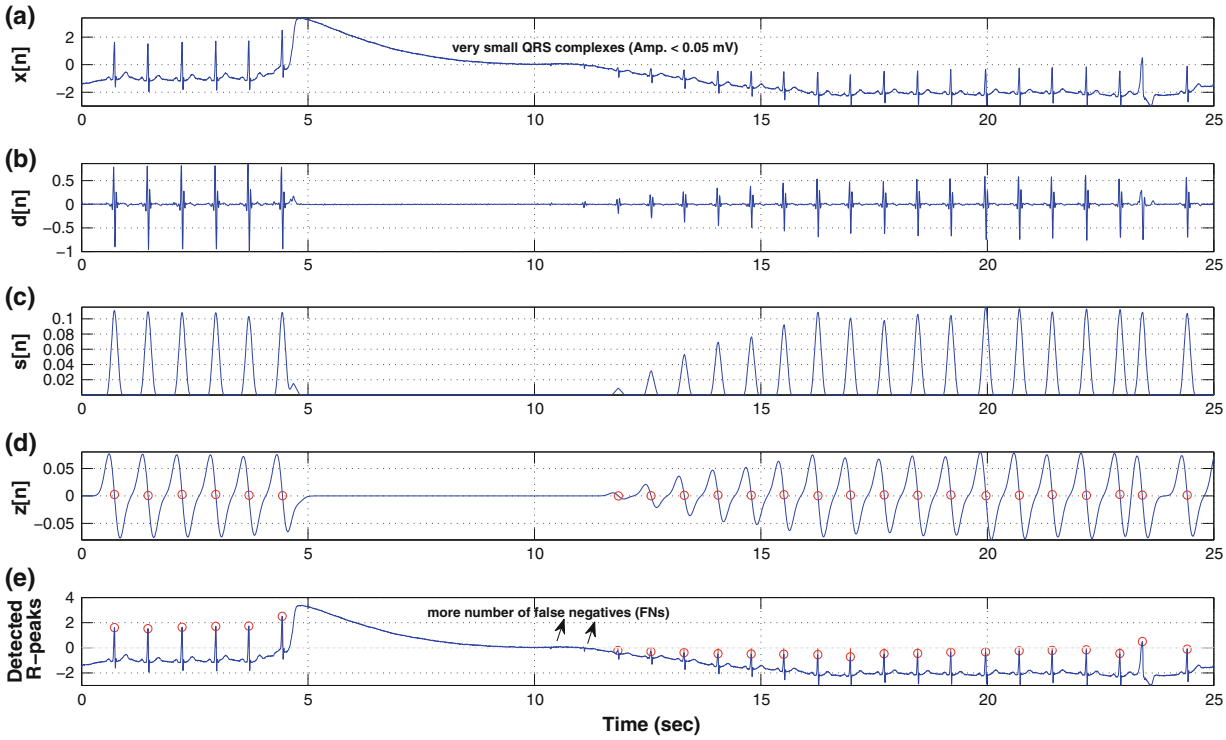

FIGURE 8. Detection performance for the ECG record 116 with very small QRS complexes (Amp. <0.05 mV). The algorithm produces 18 missed beats for a total of 2412 true beats.

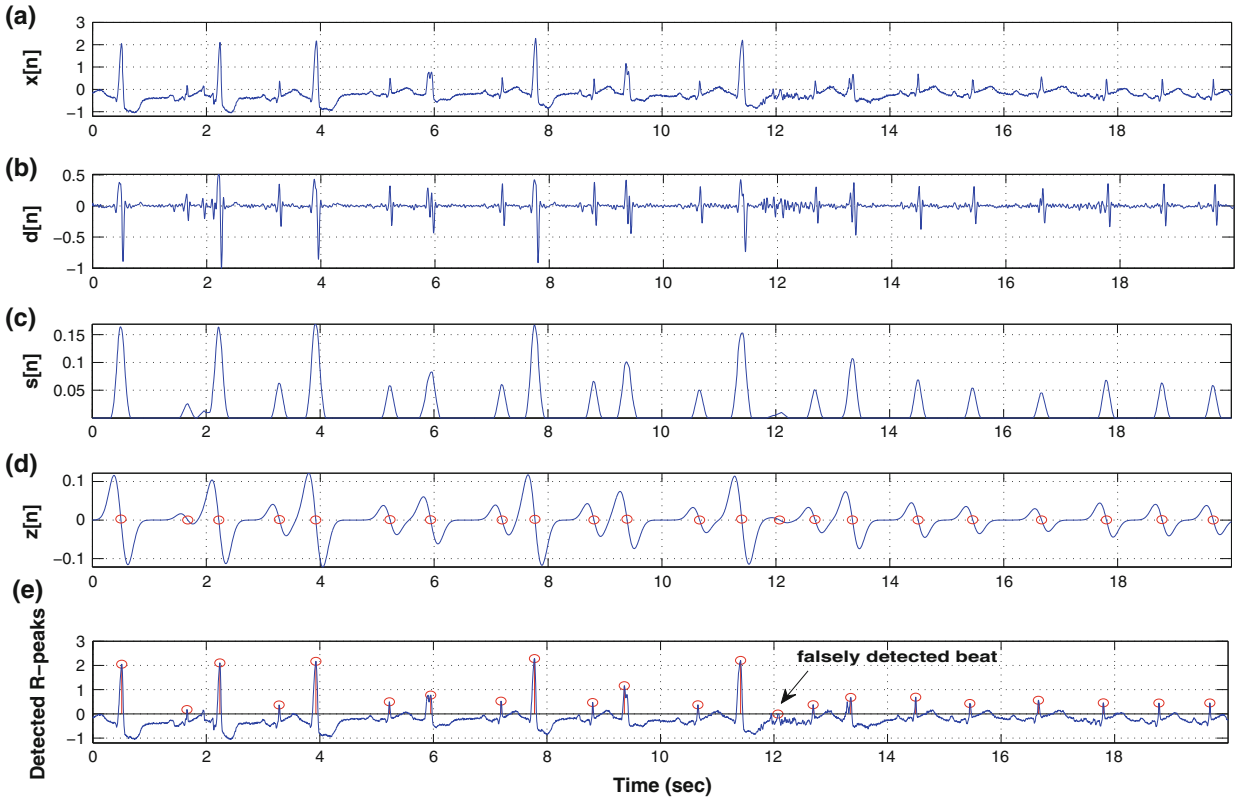

FIGURE 9. Detection performance for the ECG record 228 with very big change in amplitudes of adjacent R-peaks and severe noise. Our algorithm produces 10 FP beats and 2 FN beats for a total of 2053 true beats.

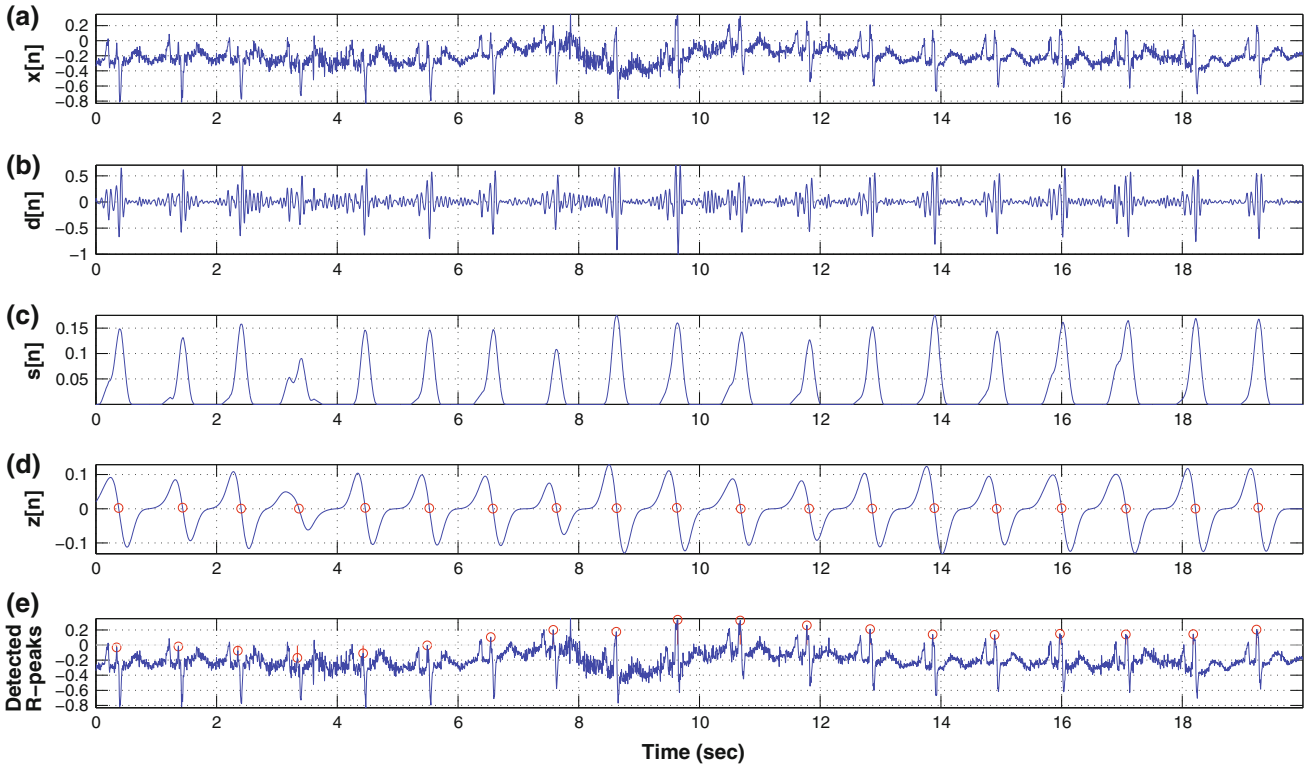

FIGURE 10. Detection performance for the ECG record 108 with large P-waves and severe muscle noise. Our algorithm produces four FP beats and one FN beats for a total of 1763 true beats.

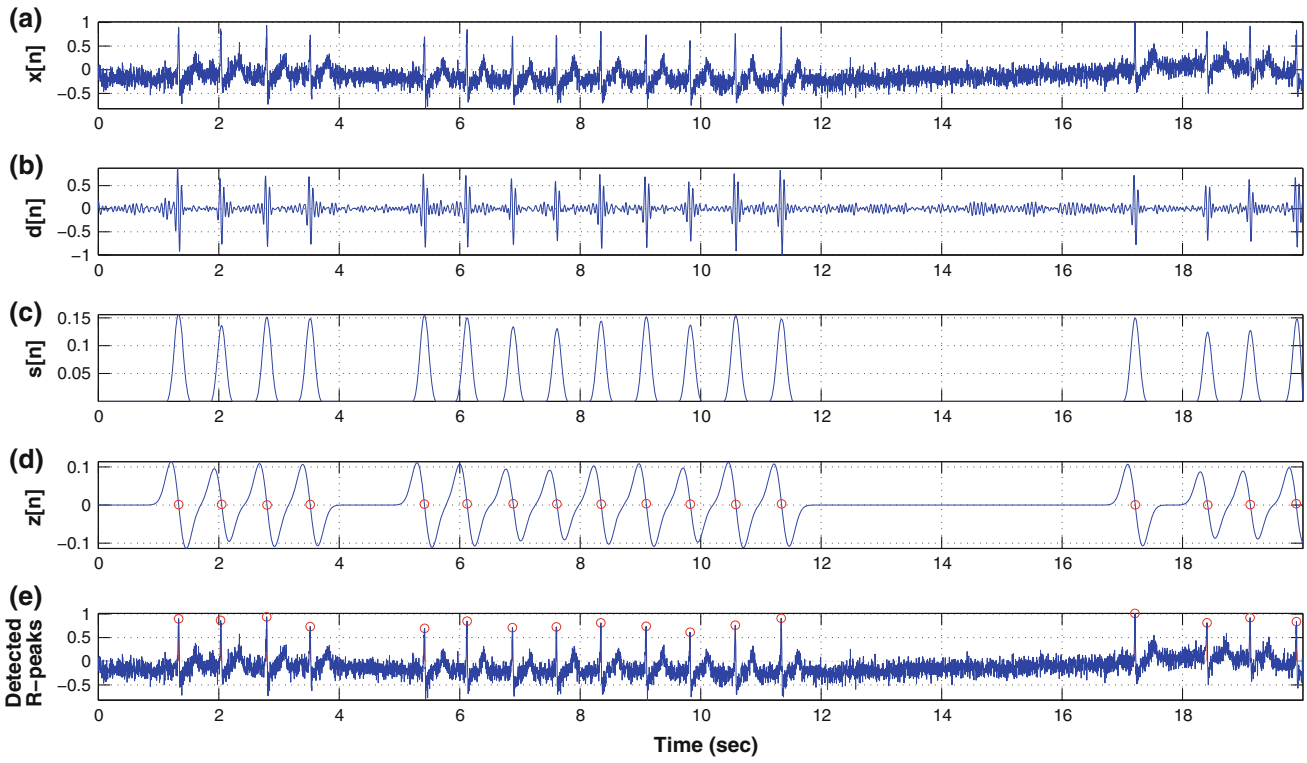

FIGURE 11. Detection performance for the ECG record 232 with noise and numerous long pauses up to 6 s. Our algorithm produces 2 FP beats and 0 FN beats for a total of 1780 true beats.

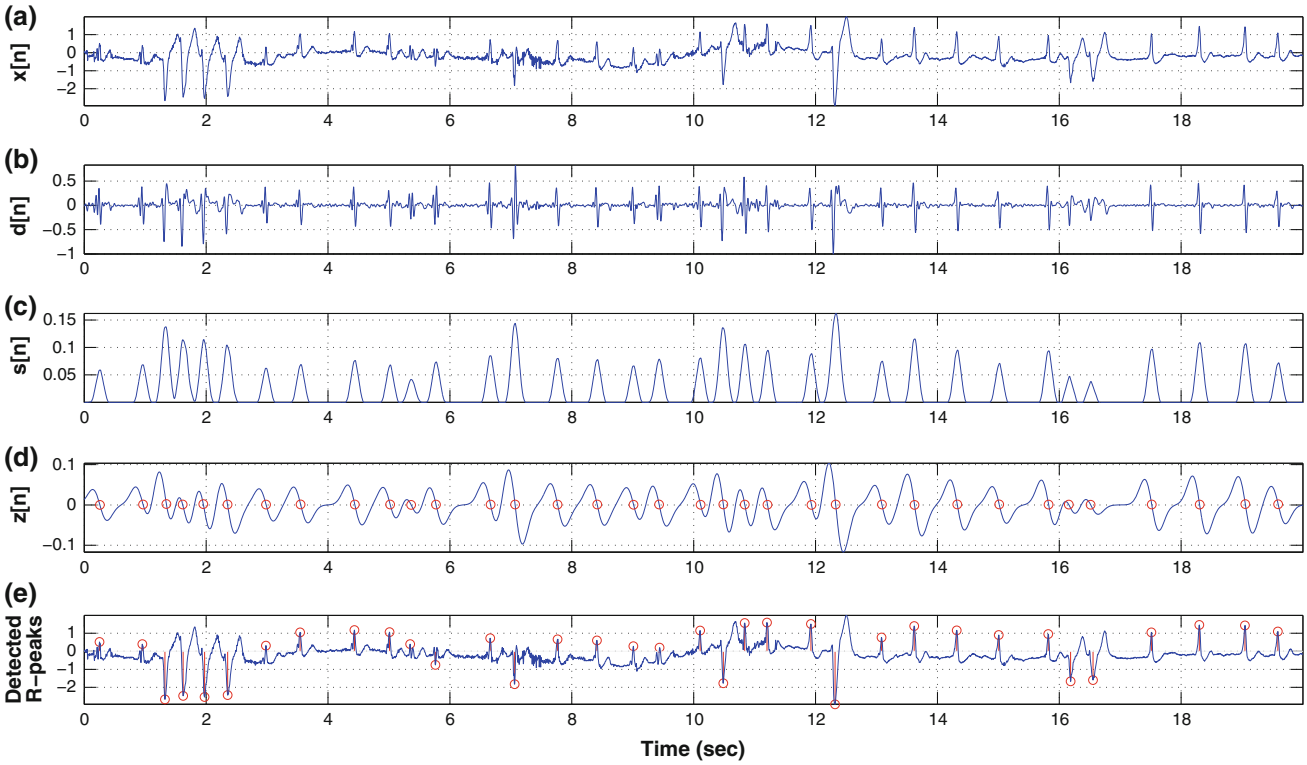

FIGURE 12. Detection performance for the ECG record 203 with very big change in adjacent QRS-shape, QRS-amplitude and heart rates, many short RR-interval (RR <360 ms), very small QRS (Amp. <0.04 mV), and noise and artifacts. This is a very difficult record, even for humans. Our algorithm produces 2 FP beats and 14 FN beats for a total of 2980 true beats.

peak-finding technique achieves higher detection accuracy, easy to implement, and provides the significant computational advantage as compared to that of Hilbert transform-based peak technique reported in our previous work in Sabarimalai Manikandan and Dandapat.[30] The most common ECG abnormality is the presence of low amplitude QRS complexes, probably due to myocardial infiltration-for example, amyloidosis, sarcoidosis, and haemochromatosis. Most commonly, a wide QRS complex is due to abnormal conduction over the right or left bundle due to block or delay of ventricular activation. The PVCs are caused by heart attack, and are characterized by premature and bizarrely shaped QRS complexes usually having wider duration of greater than 120 ms.

The overall performance of the various QRS detection methods is summarized in Table 5. In the literature, many methods had more false negative detections for the ECG records namely 200, 201, 203, 208, and 228 that include small-QRS complexes, wide-QRS complexes and very big change in adjacent QRS-shape, QRS-amplitude, and heart rates. The accuracy of computer-aided cardiac diagnostic system may be degraded due to missed or falsely detected beats. For example, misclassification of beats is more problematic in heart rate variability, ECG wave delineator, fHRM, cardiac sound separator, patient authentication and ECG coder.

Various experiments prove that the proposed nonlinear transformation and simple peak-finding techniques improves the detection performance. The experimental results demonstrate that the proposed algorithm has lower false-positive and false-negative rates in the case of ECG signals with sharp and tall P and T waves, negative QRS complex, small QRS complex, wider QRS complex, muscle noise, baseline drift, sudden changes in QRS amplitudes, sudden changes in QRS morphology, multiform PVCs, long pauses and irregular heart rhythms.

CONCLUSION

This paper presents a new and simple algorithm for automatically detecting R-peaks in a ECG signal. The algorithm consists of new nonlinear transformation and simple peak-finding techniques. The proposed nonlinear transformation is based on energy thresholding, Shannon energy computation, and smoothing process. This nonlinear transformation process reduces the number of false-positives and false-negatives in the case of ECG signal with small-QRS and wide-QRS

complexes, and noises. In this work, we also developed a simple peak-finding technique using the FOGD. The proposed peak-finding technique automatically determines locations of candidate R-peaks in the QRS feature signal. The proposed R-peak detection algorithm is validated using all 48 half-hour ECG records from the MIT-BIH arrhythmia database and achieves an average sensitivity of 99.94%, and a positive predictivity of 99.96%. The proposed algorithm produces 38 false positive beats and 76 false negative beats for a total 109,496 true ECG beats. Experimental results show that this algorithm outperforms other existing algorithms in case of pathological and noisy signals. The main advantages of the proposed algorithm compared with the other existing algorithms are that (1) it is a one-pass algorithm without any further searchback algorithm, (2) it uses a single thresholding rule, (3) it uses simple peak-finding strategy, and (4) it does not require sets of thresholds based upon the R peaks and RR intervals that are determined in the previous segment, a set of medical tactics to reduce false-positives and detect missed beats, and learning phase. Thus, the proposed algorithm is more suitable for automated ECG signal analysis applications.

ACKNOWLEDGMENTS

The authors would like to thank Editor-in-Chief, for his continuous encouragement and the anonymous referees for their valuable suggestions and comments.

REFERENCES

[1]Abdelliche, F., and A. Charef. R-peak detection using a complex fractional wavelet. In: International Conference on Electrical and Electronics Engineering, Bursa, 2009, pp. 267–270.

[2]Abibullaev, B., and H. D. Seo. A new QRS detection method using wavelets and artificial neural networks. *J. Med. Syst*. 2010. doi:10.1007/s10916-009-9405-3.

[3]Adnane, M., Z. Jiang, and S. Choi. Development of QRS detection algorithm designed for wearable cardiorespiratory system. *Comput. Methods Programs Biomed*. 93(1):20–31, 2009.

[4]Arzeno, N. M., Z.-D. Deng, and C.-S. Poon. Analysis of first-derivative based QRS detection algorithms. *IEEE Trans. Biomed. Eng*. 55(2):478–484, 2008.

[5]Benitez, S., P. A. Gaydecki, A. Zaidi, and A. P. Fitzpatrick. The use of the Hilbert transform in ECG signal analysis. *Comput. Biol. Med*. 31:399–406, 2001.

[6]Biel, L., O. Pettersson, L. Philipson, and P. Wide. ECG analysis: a new approach in human identification. *IEEE Trans. Instrum. Meas*. 50(3):808–812, 2001.

[7]Chen, Y. L., and H. L. Duan. A QRS complex detection algorithm based on mathematical morphology and envelope. In: Proceedings of 27th Annual International Conference of the IEEE EMBS, Shanghai, China, 2005, pp. 4654–4657.

[8]Darrington, J. Towards real time QRS detection: a fast method using minimal pre-processing. *Biomed. Signal Process. Control* 1:169–176, 2006.

[9]Elgendi, M., M. Jonkman, and F. De Boer. R wave detection using Coiflets wavelets. In: IEEE 35th Annual Northeast Bioengineering Conference, Boston, MA, 2009, pp. 1–2.

[10]El-Segaier, M., O. Lilja, S. Lukkarinen, L. Srnmo, R. Sepponen, and E. Pesonen. Computer-based detection and analysis of heart sound murmur. *Ann. Biomed. Eng*. 33(7):937–942, 2005.

[11]Gerencsr, L., G. Kozmann, and H. K. Zsuzsanna. The use of the SPSA method in ECG analysis. *IEEE Trans. Biomed. Eng*. 49(10):1094–1101, 2002.

[12]Ghaffari, A., H. Golbayani, and M. Ghasemi. A new mathematical based QRS detector using continuous wavelet transform. *Comput. Electr. Eng*. 34:81–91, 2008.

[13]Hadj Slimane, Z.-E., and A. Nait-Ali. QRS complex detection using empirical mode decomposition. *Digit. Signal Process. Rev. J*. 20(4):1221–1228, 2010.

[14]Hamilton, P. S., and W. J. Tompkins. Quantitative investigation of QRS detection rules using the MIT/BIH arrhythmia database. *IIEEE Trans. Biomed. Eng*. 33:1157–1165, 1986.

[15]Hongyan, X., and H. Minsong. A new QRS detection algorithm based on empirical mode decomposition. In: Proceedings of the 2nd International Conference on Bioinformatics and Biomedical Engineering, 2008, pp. 693–696.

[16]Huang, B., and Y. Wang, Detecting QRS complexes of two-channel ECG signals by using combined wavelet entropy. In: International Conference on Bioinformatics and Biomedical Engineering, Beijing, China, 2009, pp. 1–4.

[17]Hughes, N. P. Probabilistic models for automated ECG interval analysis. PhD thesis, University of Oxford, 2006.

[18]Kadambe, S., R. Murray, and G. F. B. Bartels. Wavelet transform-based QRS complex detector. *IEEE Trans. Biomed. Eng*. 46(7):838–848, 1999.

[19]Karvounis, E. C., M. G. Tsipouras, D. I. Fotiadis, and K. K. Naka. An automated methodology for fetal heart rate extraction from the abdominal electrocardiogram. *IEEE Trans. Inf. Technol. Biomed*. 11(6):628–638, 2007.

[20]Khler, B.-U., C. Hennig, and R. Orglmeister. The principles of software QRS detection. *IEEE Eng. Med. Biol. Mag*. 21:42–57, 2002.

[21]Kligfield, P., L. S. Gettes, and J. J. Bailey. Recommendations for the standardization and interpretation of the electrocardiogram: part I. The electrocardiogram and its technology: a scientific statement from the American Heart Association Electrocardiography and Arrhythmias Committee, Council on Clinical Cardiology; the American College of Cardiology Foundation; and the Heart Rhythm Society endorsed by the International Society for Computerized Electrocardiology. *Heart Rhythm* 4(3):394–412, 2007.

[22]Li, C., C. Zheng, and C. Tai. Detection of ECG characteristic points using wavelet transforms. *IEEE Trans. Biomed. Eng*. 42:21–28, 1995.

[23]Martnez, J. P., R. Almeida, S. Olmos, A. P. Rocha, and P. Laguna. A wavelet-based ECG delineator: evaluation on standard databases. *IEEE Trans. Biomed. Eng*. 51(4):570–581, 2004.

[24]Meyer, C., J. F. Gavela, and M. Harris. Combining algorithms in automatic detection of QRS complexes in ECG signals. *IEEE Trans. Inf. Technol. Biomed.* 10(3):468–475, 2006.
[25]Pahlm, O., and L. Srnmo. Software QRS detection in ambulatory monitoring—a review. *Med. Biol. Eng. Comput*. 22:289–297, 1984.
[26]Pan, J., and W. J. Tompkins. A real time QRS detection algorithm. *IEEE Trans. Biomed. Eng*. 32(3):230–236, 1985.
[27]Prasanna, S. R. M., and A. Subramanian. Finding pitch markers using first order Gaussian differentiator. In: IEEE Proceedings of the Third International Conference on Intelligent Sensing Information Process, 2005, pp. 140–145.
[28]Romero, L., P. S. Addison, and N. Grubb. R-wave detection using continuous wavelet modulus maxima. *IEEE Proc. Comput. Cardiol*., 30:565–568, 2003.
[29]Sabarimalai Manikandan, M., and S. Dandapat. Wavelet threshold based TDL and TDR algorithms for real-time ECG signal compression. *Biomed. Signal Process. Control* 3:44–66, 2008.
[30]Sabarimalai Manikandan, M., and S. Dandapat. A novel method for detecting R-peaks in eletrocardiogram (ECG) signal. *Biomed. Signal Process. Control*, 2011. doi: 10.1016/j.bspc.2011.03.004.
[31]Surez, K. V., J. C. Silva, Y. Berthoumieu, P. Gomis, and M. Najim. ECG beat detection using a geometrical matching approach. *IEEE Trans. Biomed. Eng*. 54(4):485–489, 2007.
[32]Tang, J., X. Yang, J. Xu, Y. Tang, Q. Zou, and X. Zhang. The algorithm of R Peak detection in ECG based on empirical mode decomposition. In: Fourth International Conference on Natural Computation, 2008, Vol. 5, pp. 624–627.
[33]Thakor, N. V., J. G. Webster, and W. J. Tompkins. Estimation of QRS complex power spectra for design of a QRS filter. *IEEE Trans. Biomed. Eng*. 31:702–706, 1984.
[34]Trahanias, P. E. An approach to QRS complex detection using mathematical morphology. *IEEE Trans. Biomed. Eng*. 40(2):201–205, 1993.
[35]Y.-C. Yeha, and W.-J. Wanga. QRS complexes detection for ECG signal: the difference operation method. *Comput. Methods Programs Biomed*. 91:245–254, 2008.
[36]Zhang, F., and Y. Lian. QRS detection based on multiscale mathematical morphology for wearable ECG devices in body area networks. *IEEE Trans. Biomed. Circuits Syst*. 3(4):220–228, 2009.
[37]Zhang, F., and Y. Lian. QRS detection based on morphological filter and energy envelope for applications in body sensor networks. *J. Signal Process. Syst*., 2009. doi: 10.1007/s11265-009-0430-8.
[38]Zhu, W., H. Zhao, and X. Chen. A new QRS detector based on empirical mode decomposition. In: IEEE 10th International Conference on Signal Processing (ICSP), 2010, pp. 1–4.